Colloidal micromotor in smectic A liquid crystal driven by DC electric field†

Antal Jákli,* Bohdan Senyuk, Guangxun Liao and Oleg D. Lavrentovich

Received 8th May 2008, Accepted 23rd July 2008
First published as an Advance Article on the web 15th October 2008
DOI: 10.1039/b807927g

Converting linear stimulus to rotation has endless examples in virtually all scales of the universe. One of the interesting examples is Quincke rotation, a spinning rotation of a dielectric sphere neutrally buoyant in an isotropic fluid caused by a unidirectional DC electric field. Recently Quincke rotation has been reported in liquid crystalline (LC) phases, and it was noted that spinning triggers a translational motion normal to the electric field and the rotation axis. In this work, we explain the translation of spinning spheres as a result of hydrodynamic interaction with the bounding walls. We also describe a unique orbiting motion: the spinning particles circumnavigate air inclusions in the liquid crystal. The effect is caused by an elastic entrapment of the spheres at tilted grain boundaries in the meniscus region in the smectic phase. This phenomenon can offer new types of microfluidic devices and micromotors.

1 Introduction

One of the interesting examples of various forms of conversions of linear stimulus to rotation is Quincke rotation:[1,2] a unidirectional DC electric field causes a spinning rotation of a dielectric particle neutrally buoyant in an isotropic fluid. The physics of the phenomenon is related to differences in the characteristic times of electric charge relaxation within the particle and in the surrounding fluid.[3] If the first is longer than the second one, the effective electric dipole created by free electric charges accumulated at the particle–fluid interface is anti-parallel to the applied DC field. Such an orientation is unstable and, if the field is sufficiently high to overcome the viscous friction, the particle starts to spin. In absence of shear flow, the spin direction is arbitrary in the plane perpendicular to the electric field. Recently Quincke rotation has been reported for the liquid crystalline phases, *i.e.*, fluids with orientational order.[4] The orientational order and associated anisotropic elastic, viscous, dielectric and electroconductivity properties of liquid crystal (LC) fluids make phenomena such as Quincke rotation much richer than in isotropic fluids. Experimentally, Quincke rotation was observed for cylinders and spheres in the LC slab confined between two plates with conducting transparent electrodes.[4] It was also noticed that at some field above the Quincke spinning threshold, the particles start to experience a translational motion, mostly in the plane perpendicular to the applied electric field. In the smectic A phase, this translational motion is mostly confined to the 2D planes of the smectic layers; translations in the nematic and isotropic phases have arbitrary directions. Similar electromigration can also be caused in liquid crystals by an AC field,[5–8] but in those cases the spinning of the particles has not been established and the translation is generally associated with the backflow mechanism. Since the translation of Quincke rotators was observed not only in the liquid crystalline phases, but also in the isotropic phase,[4] we propose that the translation is due to a hydrodynamic interaction between the rotating particle and the bounding wall of the sample.

In this work first we will present a simple theory that explains the electro-rotation and the ensuing translation of the particles in a bound fluid, then we will describe a unique mode of the translational motion of Quincke rotators, namely their orbiting rotation around air bubble inclusions. This phenomenon exists only in the smectic A liquid crystals and is not observed (within the range of the explored experimental limits) in the nematic and isotropic phases. Our analysis of the translation effect suggests that the orbiting motion is due to defects in the layered structure of the smectic A, which trap the migrating particles and convert their spin and translation into orbiting rotation along the circularly shaped defect regions around the bubble inclusions. This phenomenon can offer new types of liquid crystalline microfluidic devices or micromotors.

2 Experimental

We have studied the commercially available LC material octyl cyano biphenyl (8CB) from Aldrich in 6 μm$<d<$70 μm thick cells with homeotropic alignment (the director is perpendicular and smectic layers are parallel to the substrates) with polarizing optical microscopy (POM) and fluorescent confocal polarizing microscopy[9] (FCPM). Details of the cell preparation and optical methods are described in the ESI.† 8CB has a smectic A (SmA) phase between 21 °C and 33 °C, and a nematic (N) phase from 33 °C up to 40.5 °C, where it becomes an isotropic (Iso) fluid. Glass spheres[10] of diameter 4.5 μm were added at low concentrations (<0.1 volume%). The mixture was filled between plane-parallel glass substrates coated with transparent indium tin oxide (ITO) electrodes.

3 Results and discussion

As described earlier,[4] at voltages above some threshold, the spheres start to spin around a horizontal axis and translate in the plane of the cell. In a homogeneous sample the translation is random. However, in the SmA phase, most of the randomly

Liquid Crystal Institute and Chemical Physics Interdisciplinary Program, Kent State University, Kent, OH 44242, USA. E-mail: jakli@lci.kent.edu
† Electronic supplementary information (ESI) available: Methods and structural characterization of studied system. See DOI: 10.1039/b807927g

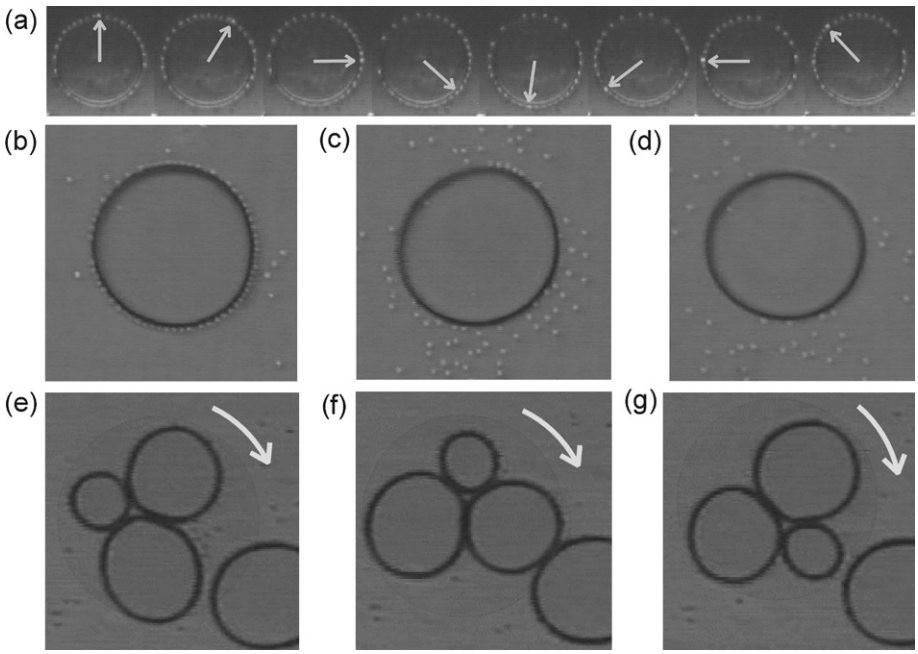

Fig. 1 Rotation in SmA under a DC electric field: (a) orbital rotation of 4.5 μm glass spheres around a 90 μm air bubble in the SmA phase of 8CB at 31 °C under the DC electric field normal to the plane of the figure. Snapshots were taken every 1/3 s. Arrows point one of the glass spheres rotating clockwise around the bubble. Middle row: arrangement of spheres around the air bubble in (b) SmA phase (31 °C), (c) N phase (34 °C), and (d) Iso phase (41 °C). Bottom row: clockwise rotation (curved arrows indicate the sense of rotation) of aggregated air bubbles (highlighted by a circle) at $U = 70$ V applied to 10 μm SmA cell: (e) $t = 0$ s; (f) $t = 1$ s; (g) $t = 2$ s. All textures are taken under the polarizing microscope with crossed polarizers; in (b)–(g), a wave-plate has been inserted in the optical pathway. Motion pictures of corresponding textures are available in the ESI.†

migrating particles became trapped by air bubbles (Fig. 1) when they hit the air bubble directly or pass within a few micrometres of it. In time, the number of trapped particles increases and they orbit the bubbles in a synchronized manner (see Fig. 1 and ESI†). The orbiting motion is either clockwise or anticlockwise, but once it is established it does not change sign until the field is on. Upon heating the sample to the N (Fig. 1c) or Iso (Fig. 1d) phase, the particles detach from the air bubbles and travel through the entire sample. When two or three single particles meet, they stick together and rotate around their center of gravity. In areas where the density of the air bubbles is high, the bubbles may stick together and rotate about their center of gravity (see Fig. 1e–g and ESI†). The angular velocities of the air bubble aggregates are much smaller than that of the particles.

The linear velocity of the synchronized orbital motion of spheres, measured as a function of applied voltage, shows a threshold behavior (Fig. 2a). The speed does not depend on the diameter of the air bubbles within the measurement error, and is basically equal to the speed of the non-trapped particles.

FCPM (Fig. 3) reveals that the colloidal particles are located in the LC bulk. The reason for this "levitation" is that the gravity forces (~0.6 pN for 4.5 μm glass spheres) are balanced by the elastic director distortion forces (~10 pN, see ref. 8). The particles orbiting the air inclusions are located in the meniscus regions but touch neither the substrate nor the free surface (see Fig. 3a and c). The meniscus contact angle $\theta > 20^\circ$ does not change measurably in the electric field. The meniscus necessitates a tilted grain boundary[11,12] (TiGB), as the surface anchoring keeps the SmA layers parallel to both the rigid wall and air–smectic interface.

Quincke rotation in DC fields occurs if the electric charge relaxation time within the particle is larger than in the surrounding liquid[3,13] because the effective electric dipole created by free electric charges accumulated at the particle–fluid interface becomes anti-parallel to the applied DC field. Such an orientation is unstable and, if the applied voltage U is sufficiently high, the particle starts to spin with an angular velocity[3,13] $\Omega = \pm\frac{1}{\tau_{MW}}\sqrt{\frac{U^2}{U_c{}^2} - 1}$. Here U_c is the threshold of rotation,[14] $\upsilon_{MW} = \varepsilon_0(\varepsilon_s + 2\varepsilon_l)/(\sigma_s + 2\sigma_l)$ is the Maxwell–Wagner relaxation time, ε_s (ε_l) and σ_s (σ_l) are the relative dielectric permittivities and the conductivities of the solid particle (liquid medium), ε_0 is permittivity of free space. If $\sigma_l >> \sigma_s$, then $U_c = \sqrt{\frac{8\mu\sigma_l}{3\varepsilon_0{}^2\varepsilon_l\varepsilon_s}}d$ and $\Omega = \pm\frac{3U_c{}^2\varepsilon_0\varepsilon_l\varepsilon_s}{4\mu(\varepsilon_s + 2\varepsilon_l)d^2}\sqrt{\frac{U^2}{U_c{}^2} - 1}$, where μ is the viscosity of the liquid.

The experiments above reveal that the Quincke rotation is accompanied by a translational motion in the SmA, N and Iso phases. The effect has not, to the best of our knowledge, been reported in the literature (see, *e.g.*, ref. 3). Although electromigration of colloidal inclusions has been observed in LCs under the action of an AC field,[5–8] in those cases the spinning of the particles has not been established and the translation was generally associated with the backflow.[15,16] The backflow model was indeed demonstrated to provide a good description of particle translation in the nematic cells under the AC field.[8] However, the backflow mechanism is definitely not applicable for

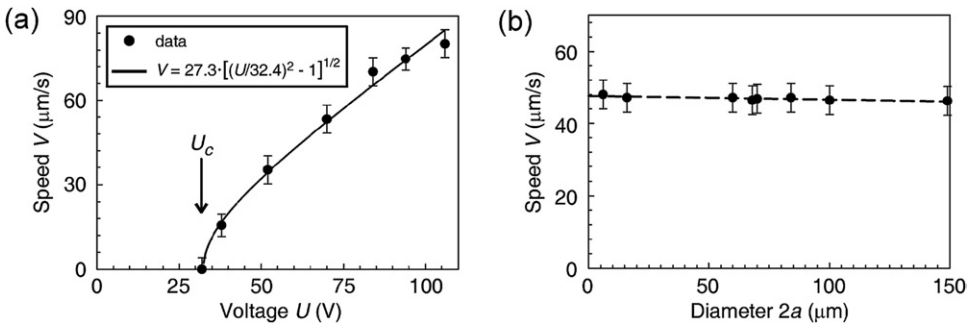

Fig. 2 Linear speed of 4.5 μm spheres in a 6 μm thick homeotropic SmA cell at 31.3 °C: (a) as a function of a DC voltage for orbiting around an air bubble of diameter 74.5 μm, and (b) as a function of air bubble diameter at constant $U = 60$ V. (The smallest diameter actually corresponds to that of glass beads stuck together, rotating around their center of gravity.)

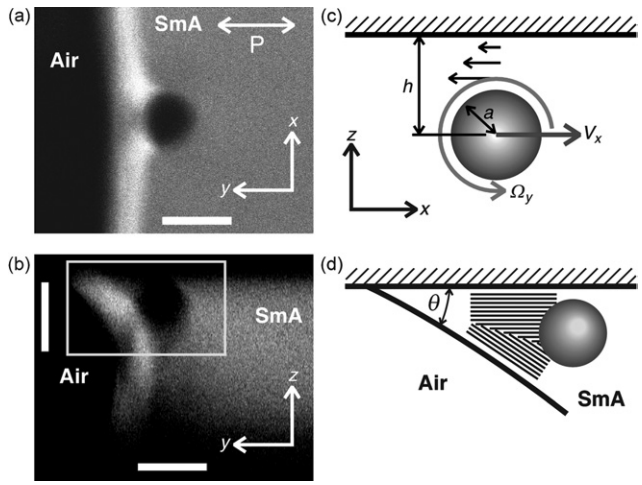

Fig. 3 Structures and solid spheres in the meniscus of SmA: (a) in-plane (xy) and (b), vertical (yz) FCPM textures of a sphere in SmA near the air bubble at room temperature. The bright zones in the meniscus region correspond to director deviations from the vertical axis z. (c) Scheme of rotation and translation of a particle near a wall. (d) TiGB with a trapped bead in the meniscus, corresponds to the region denoted by the box in (b). θ is the contact angle, V_x is the translational velocity, Ω_y is the angular velocity, h is the distance to the wall, a is the radius of the particle. "P" indicates the polarization of the probing light. The horizontal and vertical bars are 5 μm.

the case of the isotropic and SmA phases in this present work. In the isotropic phase there is no director, and in the homeotropic SmA the electric field causes no reorienting torque on the director in the regions away from the meniscus (yet the spheres translate there as well as in the meniscus).

Translation of the spinning spheres in the absence of direct contact between the particle and the boundaries can be explained by hydrodynamic interaction with the walls. The particle–wall separation is much shorter than the viscous penetration length $\zeta = \sqrt{\mu/(\rho\Omega)}$, which for typical $\Omega \approx 20$ s^{-1} (see ref. 4), 8CB viscosity $\mu \approx 1$ Pa s and density $\rho \approx 10^3$ kg m^{-3} is well over a millimetre. If the sphere spins near a planar wall at a distance $h<\zeta$, the velocity gradient between the wall and the sphere is much steeper (and thus the viscous stress is larger) than in the rest of the space (Fig. 3b), so there is a force pushing the sphere along the wall, perpendicular to the rotation axis.

To find the relationship between the angular velocity of spinning Ω_y around the y-axis and the linear velocity V_x parallel to the wall, in the regime of small Reynolds number, we consider the linear balance of forces and torques acting on the sphere: $F^{\mathrm{t}}_x + F^{\mathrm{r}}_x = 0$, $T^{\mathrm{E}}_y + T^{\mathrm{t}}_y + T^{\mathrm{r}}_y = 0$. Here $F^{\mathrm{t}}_x = 6\pi\mu a V_x F^{\mathrm{t}}_x{}^*$ and $F^{\mathrm{r}}_x = 6\pi\mu a^2 \Omega_y F^{\mathrm{r}}_x{}^*$ are the viscous forces associated with translation and rotation, respectively; $T^{\mathrm{t}}_y = 8\pi\mu a^2 V_x T^{\mathrm{t}}_y{}^*$ and $T^{\mathrm{r}}_y = 8\pi\mu a^3 \Omega_y T^{\mathrm{r}}_y{}^*$ are the corresponding viscous torques and $T^{\mathrm{E}} = 8\pi\mu a^3 \dfrac{\Omega_y}{1+\tau_{\mathrm{MW}}{}^2\Omega_y{}^2}\dfrac{U^2}{U_{\mathrm{c}}{}^2}$ is the torque imparted by the electric field.[3] The numerical coefficients $F^{\mathrm{t}}_x{}^*$, $F^{\mathrm{r}}_x{}^*$, $T^{\mathrm{t}}_y{}^*$ and $T^{\mathrm{r}}_y{}^*$ are functions of the ratio a/h, accounting for the effect of the wall, with the values $F^{\mathrm{t}}_x{}^* = -\left[1 - \dfrac{9}{16}\dfrac{a}{h} + \dfrac{1}{8}\left(\dfrac{a}{h}\right)^3\right]^{-1}$, $F^{\mathrm{r}}_x{}^* = \dfrac{3}{32}\left(\dfrac{a}{h}\right)^4$, $T^{\mathrm{t}}_y{}^* = \dfrac{3}{4}F^{\mathrm{r}}_x{}^*$, and $T^{\mathrm{r}}_y{}^* = -1 - \dfrac{5}{16}\left(\dfrac{a}{h}\right)^3$ when $a/h << 1$.[17] The model does not consider forces along the z-axis, such as hydrodynamic,[18] electrokinetic[19] or elastic[8] lift forces, and neglects all boundaries except the closest solid wall. The solution is

$$V_x = \frac{1}{8}a\Omega_y\left(\frac{a}{h}\right)^4;$$
$$\Omega_y = \pm\frac{3U_{\mathrm{c}}{}^2\varepsilon_0\varepsilon_1\varepsilon_{\mathrm{s}}}{4\mu(\varepsilon_{\mathrm{s}}+2\varepsilon_1)d^2}\sqrt{\left(\frac{U}{U_{\mathrm{c}}}\right)^2\left[1-\frac{5}{16}\left(\frac{a}{h}\right)^3\right]-1}. \quad (1)$$

Eqn (1) captures the essential features of the experiment, namely, that a Quincke rotator in the presence of a wall experiences a translation with linear velocity $V_x(U)$ that fits the data in Fig. 2b well. Experimentally, $U_{\mathrm{c}} = 32$ V (Fig. 1a), $\varepsilon_{\mathrm{s}} = 3.9$, $\mu = 1.6$ Pa s (see ref. 4) and $\varepsilon_{\mathrm{s}}/2\varepsilon_1 \approx 0.15$, so that $\dfrac{3U_{\mathrm{c}}{}^2\varepsilon_0\varepsilon_1\varepsilon_{\mathrm{s}}}{4\mu(\varepsilon_{\mathrm{s}}+2\varepsilon_1)d^2} \approx 200$ s^{-1} and $\dfrac{V_x}{a\Omega_y} \approx 0.06$, clearly smaller than the "rolling limit" $\dfrac{V_x}{a\Omega_y} = 1$. In the model, $\dfrac{V_x}{a\Omega_y} \approx \dfrac{1}{8}\left(\dfrac{a}{h}\right)^4$, which implies that $a/h \approx 0.8$ which is reasonable based on our FCPM observations (Fig. 3). Although it might be too large to justify the approximation $a/h << 1$, the comparison of analytic and numerical results for a similar problem of translating and rotating a sphere in a shear flow[20] shows that even for $a/h = 0.96$ the

relative error is only[21] ~10%. One should not expect a better agreement also because the spheres orbiting the meniscus are hydrodynamically influenced by the other trapped spheres,[22] which is neglected in the calculations.

The orbiting motion of the spheres in SmA is a result of the translational motion and the elastic entrapment of particles at TiGB in the meniscus region. A TiGB naturally confines the trajectories of the spheres moving parallel to the SmA layers. Moving a particle from a uniform SmA region into the TiGB decreases the elastic distortion energy[23] by $\sim a^2\Phi$, where $\Phi \approx K/\lambda$, with $K \approx 1 \times 10^{-11}$, N being the elastic constant of the director splay and $\lambda \approx 1$ nm is the "penetration length" of SmA.[11] The corresponding "trapping" force $F_{\mathrm{trap}} \approx a\Phi \approx K\frac{a}{\lambda} \approx 10^{-8}N$ is much larger than the centrifugal force $F_c = (4/3)a^3\pi\rho V^2/b \approx 10^{-17}N$, as estimated for a bubble radius $b \approx 50$–100 μm and speed $V \approx 100$ μm s^{-1}.

The spinning axis of an orbiting sphere might fluctuate and thus redirect the spin-induced propulsion force. The sphere would leave the meniscus region if its velocity in the radial (with respect to the air bubble) direction is high enough to overcome the elastic trapping forces. This maximum velocity can be estimated by equating F_{trap} to the viscous force $F \approx 6\pi\mu aV$: $V_{\max} \approx \frac{K}{\lambda}\frac{1}{6\pi\mu} \approx 500$ μm s^{-1} for $\mu \approx 1$ Pa s, which is well above the typical velocity in our experiments. In the N phase, the director distortions spread over a macroscopic distances ξ, and the trapping force becomes[23] $F_t^N \approx K\left(\frac{a}{\xi}\right)^3$. Taking $\xi \approx a$ and $\mu \approx 0.1$ Pa s, one finds $V_{\max} \approx \frac{K}{a}\frac{1}{6\pi\mu} \approx 2$ μm s^{-1}, smaller than the experimental V_x, which explains why the spheres do not keep orbiting in the N phase. In the isotropic phase, the elastic mechanism of trapping is absent and we do not observe any trapping.

4 Conclusion

We have described a unique orbiting motion of spherical colloidal particles in a smectic LC under a DC electric field. The effect is due to the field induced Quincke rotation that triggers translation of spheres through hydrodynamic interaction with the bounding walls. In the SmA phase, the sphere can be trapped in the regions with strong director distortions and forced to follow a pre-determined pathway, such as a meniscus of the air bubble inclusions. The effect can be used in practical applications, such as micromotors.

Acknowledgements

This work has been supported by NSF DMS-0456221, DMR-0504516 and DOE DE-FG02-06ER. We acknowledge useful discussions with J.R. Kelly and I. I. Smalyukh.

References

1 W. Weiler, *Z. Phys. Chem. Unterricht*, 1893, **Heft IV**, 194–195.
2 G. Quincke, *Ann. Phys. Chem.*, 1896, **59**, 417–486.
3 T. B. Jones, *IEEE Trans. Ind. Appl.*, 1984, **20**, 845–849.
4 G. Liao, I. I. Smalyukh, J. R. Kelly, O. D. Lavrentovich and A. Jákli, *Phys. Rev. E*, 2005, **72**, 031704.
5 I. Dierking, G. Biddulph and K. Matthews, *Phys. Rev. E*, 2006, **73**, 011702; I. Dierking, P. Cass, K. Syres, R. Cresswell and S. Morton, *Phys. Rev. E*, 2007, **76**, 021707.
6 T. Togo, K. Nakayama, M. Ozaki and M. Yoshino, *Jpn. J. Appl. Phys.*, 1997, **36**, L1520; K. Nakayama, M. Ozaki and K. Yoshino, *Mol. Cryst. Liq. Cryst.*, 1999, **329**, 129–135.
7 Y. Mieda and K. Furutani, *Appl. Phys. Lett.*, 2005, **86**, 101901; Y. Mieda and K. Furutani, *Phys. Rev. Lett.*, 2005, **95**, 177801.
8 O. P. Pishnyak, S. Tang, J. R. Kelly, S. V. Shiyanovskii and O. D. Lavrentovich, *Phys. Rev. Lett.*, 2007, **99**, 127802.
9 I. I. Smalyukh, S. V. Shiyanovskii and O. D. Lavrentovich, *Chem. Phys. Lett.*, 2001, **336**, 88–96; S. V. Shiyanovskii, I. I. Smalyukh and O. D. Lavrentovich, in *Defects in Liquid Crystals: Computer Simulations, Theory and Experiments*, ed. O. D. Lavrentovich, P. Pasini, C. Zannoni, and S. Zumer, NATO Science Series, II: Mathematics, Physics and Chemistry, Klumer Academic Publishers, Dordrecht, 2001, vol. 43, pp. 229–270.
10 The silica spheres (brand name "Shinshikyu") are from Catalysts & Chemicals Co., Japan.
11 M. Kleman, *Lines and Walls in Liquid Crystals, Magnetic Systems and Various Ordered Media*, John Wiley & Sons, 1983.
12 M. Kleman and O. D. Lavrentovich, *Eur. Phys. J. E*, 2000, **2**, 47–57.
13 T. B. Jones, *Electromechanics of Particles*, Cambridge University Press, New York, 1995.
14 A. Cebers, *Phys. Rev. Lett.*, 2004, **92**, 034501.
15 F. Brochard, P. Pieranski and E. Guyon, *Phys. Rev. Lett.*, 1972, **28**, 1681–1683; A. Jákli and A. Saupe, *Mol. Cryst. Liq. Cryst.*, 1993, **237**, 389–398.
16 Z. Zou and N. Clark, *Phys. Rev. Lett.*, 1995, **75**, 1799–1802.
17 A. J. Goldman, R. G. Cox and H. Brenner, *Chem. Eng. Sci.*, 1967, **22**, 637–651.
18 S. I. Rubinow and J. B. Keller, *J. Fluid Mech.*, 1961, **11**, 447–459.
19 S. G. Bike and D. C. Prieve, *J. Colloid Interface Sci.*, 1995, **175**, 422–434; S. M. Tabatabaei, T. G. M. van de Ven and A. D. Rey, *J. Colloid Interface Sci.*, 2006, **301**, 291–301.
20 A. J. Goldman, R. G. Cox and H. Brenner, *Chem. Eng. Sci.*, 1967, **22**, 653–660.
21 F. Charru, E. Larrieu, J.-B. Dupont and R. Zenit, *J. Fluid Mech.*, 2007, **570**, 431–453.
22 S. Martin, M. Reichert, H. Stark and T. Gisler, *Phys. Rev. Lett.*, 2006, **97**, 248301.
23 D. Voloschenko, O. P. Pishnyak, S. V. Shiyanovskii and O. D. Lavrentovich, *Phys. Rev. E*, 2002, **65**, 060701.

